Journal of Materials Chemistry A

Accepted Manuscript

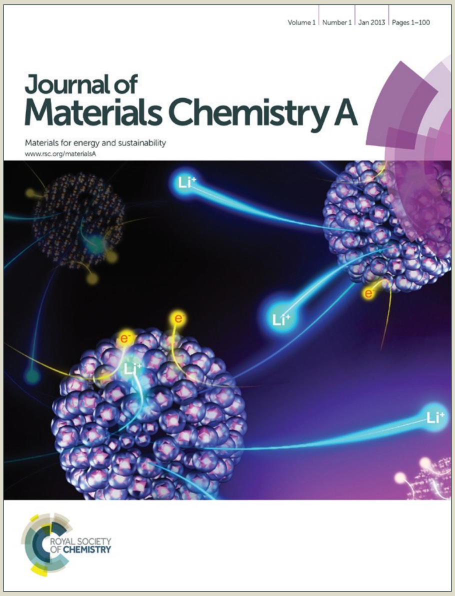

ROYAL SOCIETY OF CHEMISTRY

www.rsc.org/materialsA

Novel Au inlaid Zn_2SnO_4/SnO_2hollow rounded cubes for dye-sensitized solar cells with enhanced photoelectric conversion performance

Bo Li, EnyanGuo, Chengxiang Wang, Longwei Yin*

Key Laboratory for Liquid-Solid Structural Evolution and Processing of Materials, Ministry of Education, School of Materials Science and Engineering, Shandong University, Jinan 250061, P. R. China

*To whom correspondence should be addressed. Tel.: + 86 531 88396970. Fax: + 86 531 88396970. E-mail: yinlw@sdu.edu.cn

AbstractWe developed a facile strategy for fabrication of uniform Au inlaid Zn_2SnO_4/SnO_2 hollow rounded cubes with an adjustable Au loading content using $ZnSn(OH)_6$ as precursors, chloroauricacid as Au source and ascorbic acid as a reducing agent. The Au inlaid Zn_2SnO_4/SnO_2 hollow rounded cubes show enhanced light absorption ability and reduced recombination rate of photogenerated electron-hole pairs compared with pure Zn_2SnO_4/SnO_2. The hollow rounded cube structured Au–Zn_2SnO_4/SnO_2 sample displays a high surface area and high dye adsorption ability. As photoanodes for DSSCs, the Au-Zn_2SnO_4/SnO_2 hollow rounded cubes demonstrate a greatly enhanced J_{sc} and improved power conversion efficiency of up to 2.04%, which increase by 73% relative to photovoltaic conversion efficiency for pure Zn_2SnO_4/SnO_2 based DSSCs.The greatly improved power conversion efficiency of the DSSCs based on Au inlaid Zn_2SnO_4/SnO_2photoanode can be attributed to the following three factors. Firstly, the localized surface plasmon resonance of Au nanoparticles plays a crucial role to the enhancement of visible light absorption. Secondly, the potential barrier on the Zn_2SnO_4/SnO_2 surface caused by Au nanoparticles can suppress electron-hole recombination, diminish the loss of electrons during transfer process and improve the photocurrent density. Thirdly, the enhanced photovoltaic performance can be also attributed to unique structural characteristics of hollow rounded cubes.

Keywords: Zn_2SnO_4/SnO_2; Au nanoparticles; localized surface plasmonresonance; dye-sensitized solar cells; electron-hole pairs

1. Introduction

Dye-sensitized solar cells (DSSCs) are of great interest due to their low cost, relatively high power conversion efficiency, and their unique advantages over conventional silicon photovoltaics since the great breakthrough work by O'Regan and Gratzel in1991.[1] In the past decades, considerable efforts on novel photoanodes,[2-5] electrolytes,[6-8] and sensitizers[9-11] have been performed to improve the photovoltaic conversion efficiency and long-term stability of DSSCs.[12] The photoelectrode is one of the most important components in DSSCs, which normally is comprised of mesoporous wide-band-gap oxide semiconductor films with a high internal surface area. Thus far, majority of published works have been focused on photoanodes based on binary metal oxides such as TiO_2,[1,3-5] ZnO[13,14] and SnO_2.[15,16] Among them, TiO_2 based DSSCs have been the predominantly investigated and comprehensively employed owing to their high power conversion efficiency and low preparation cost.[4,5] However, it has been shown that TiO_2 photoanodes could cause photobleaching of the dye molecules in the UV region of the solar spectrum,[17,18] which is a major obstacle for its long-term practical applications. Alternatively, compared with simply binary materials, ternary metal oxides such as Zn_2SnO_4, $BaSnO_3$ and $SrTiO_3$ etc. offer several advantages on certain aspects.[19-21] Among multifarious ternary metal oxides, especially worth noted Zn_2SnO_4 (ZTO), has been reported to possess a band-gap of 3.6 eV and large electron mobility of 10–15 $cm^2\ V^{-1}\ s^{-1}$,[22,23] superior to that of TiO_2 (0.1-1.0 $cm^2\ V^{-1}\ s^{-1}$).[24] In addition, it can diminish photobleaching and keep long-term stability due to its wide band-gap and large band-to-band transition.[25] It is the first report on photovoltaic performance of DSSCs based on Zn_2SnO_4 nanoparticles in 2007,[26] exhibiting a superior power conversion efficiency close to the highest efficiency for ZnO fabricated qfocused on the investigations based on different morphologies of Zn_2SnO_4 such as nanowires,[27] nanoplates[28] and nanotubes.[29] Some other methods such as doping and quantum dot sensitization are also investigated to improve the power conversion efficiency of Zn_2SnO_4 photovoltaic devices.[30-33] However, insufficient visible light absorption due to its wide band-gap of 3.6eV and high recombination rate of electrons and holes still hinder the improvement of the photovoltaic performance of Zn_2SnO_4 based DSSCs.

Recently, composting different semiconductor materials to form a heterojunctionstructure to suppress the recombination rate of electron-hole pairs have been an effective route to improve the photo electrical conversion efficiency and optoelectronic performance. So far, Zn_2SnO_4/TiO_2 and Zn_2SnO_4/ZnO composite heterostructureshave been reported to show a superior photovoltaic performance compared to pure Zn_2SnO_4.[28,34] With high electron mobility of 100-200 $cm^2\ V^{-1}\ s^{-1}$, and the same band-gap of 3.6eV as that of Zn_2SnO_4, SnO_2 is also considered to be ideal photocatalytic and DSSCs material used widely.[35-37] Li et al.[38] reported DSSCs based on Zn_2SnO_4/SnO_2 composite, demonstrating that the conduction band (CB) of SnO_2 is lower than that of counterpart Zn_2SnO_4, achieving a 43% photovoltaic conversion efficiency enhancement compared with pure Zn_2SnO_4. Liu et al.[39] investigated the photocatalytic performance based on Zn_2SnO_4/SnO_2, revealing a much higher activity under solar light illumination than pure Zn_2SnO_4.

Recently, it is worthy to notethat the improvement the poor absorption of visible light can be realized by employing Localized Surface Plasmon Resonance (LSPR) of noble metal nanoparticles in DSSCs.[40-42] By proper depositing of metal nanoparticle into electrode, light can be efficiently trapped and concentrated, resulting in the optical absorption and photocurrent significantly enhanced.[43] Li et al.[44] designed a nanocomposite with Au nanoparticles inlaid in TiO_2 as working electrode, displaying a photocurrent and power conversion efficiency increase by 63% and 84%, respectively. Qi et al.[45] fabricated an Ag@TiO_2 core-shell nanostructure, achieving a photovoltaic conversion efficiency of 9.0% with reduced photoanode thickness for better electron collection. In addition to enhance light harvesting, the recombination rate of photo-generated charges of metal nanoparticle coupled semiconductor can be diminished by constituting a Schottky barrier in the interfacial region of novel metal nanoparticles and semiconductors, as demonstrated in McFarland's work.[46] When an electron in the lowest unoccupied molecular orbital of the dye tunnels is transferred to the conduction band of the semiconductor via the Au nanoparticle, it is unlikely to go back to either the dye or the electrolyte due to the presence of the Schottky barrier. However, until now, few studies have been reported on DSSCs based on ternary oxide added with novel metal nanoparticles.

For improving visible light harvesting effect to get enhanced performance of DSSCs, except for incorporating of novel metal nanoparticles, an alternative route is to make a rational microstructure design. Hollow micro/nanostructured materials have drawn growing attention owing to their high surface area to absorb dye molecules, endowing them with great potential for applications of DSSCs based on different materials such as TiO_2,[47,48] SnO_2[49,50] and ZnO.[51,52] Despite various study on DSSCs based on hollow structures so far, the light scattering effect and packing density of spherical structure are still not very sufficient due to the point-to-point contact of spherical particles.[47-51] It is reported that non-spherical hollow particles, such as nanocubes, nanoboxes, can exhibit unusual physical/chemical properties. For instance, single-/double-wall $Fe(OH)_x$ nanoboxes and CeO_2nanocubes with an average size of ~400 nm as photoanodes for DSSCs, exhibit remarkable improvement in light absorption ability and photoelectrical conversion performance.[53-54]

In this study, we develop a facile strategy for fabrication of uniform Zn_2SnO_4/SnO_2 hollow rounded cubes with an adjustable Au loading content using $ZnSn(OH)_6$ as precursors, chloroauricacid as Au source and ascorbic acid as reducing agent. The structure and morphology of Zn_2SnO_4/SnO_2 can be tuned by adjusting the concentration of NaOH, and a homogeneous deposition of Au nanoparticles on surface of Zn_2SnO_4/SnO_2 can be realized via adjusting pH value. The Au inlaid Zn_2SnO_4/SnO_2 hollow rounded cubes show enhanced light absorption ability and reduced recombination rate of photogenerated electron-hole pairs compared with pure Zn_2SnO_4/SnO_2. The enhanced photovoltaic performance and related mechanism of DSSCs based on Au-Zn_2SnO_4/SnO_2 hollow rounded cubes are evaluated. As photoanodes for DSSCs, the Au-Zn_2SnO_4/SnO_2 hollow rounded cubes demonstrate a greatly enhanced J_{sc} and improved power conversion efficiency of up to 2.04%, almost 73% higher thanthat of DSSCs based Zn_2SnO_4/SnO_2. The relation between microstructure, optical response property, electron transfer and photovoltaic performance is discussed and analyzed.

2. Experimental

2.1 Preparation of Au nanoparticles inlaid Zn_2SnO_4/SnO_2 hollow rounded cubes

Synthesis of Zn_2SnO_4/SnO_2 hollow rounded cubes

First, a typical precursor of $ZnSn(OH)_6$hollow rounded cube was synthesized through a inlaid self-templating co-precipitation method.[55] 30 mL of ethanol solution of $SnCl_4$(6 mmol) was added into 60 mL of a mixture aqueous solution containing $ZnCl_2$ (6 mmol) and citric acid (6 mmol) under stirring, followed by quick addition of 72 mmol of NaOH and150 mL of deionized water.After 10min, 120 mL of aqueous solution of NaOH (2 M) was poured into the suspension and the reaction was lasted for another 10 min. The resulting white precipitateswerecollected harvested by several rinse-centrifugation cycles with deionized water and ethanol, and dried at 60 ºC. Then the as-prepared $ZnSn(OH)_6$ hollow rounded cubeswere annealed at 800 ºC in air for 6 h with a heating rate of 2 ºC min^{-1}, resulting in a white product of Zn_2SnO_4/SnO_2hollow rounded cube.

Fabrication of Au nanoparticles inlaidZn_2SnO_4/SnO_2hollow rounded cubes

Typically, the obtained Zn_2SnO_4/SnO_2hollow rounded cubes (0.2 g) were dispersed into 150 mL aqueoussolutioncontaining 40 mg of PVP and 70 mg of ascorbic acid. This mixture was heated to 90ºC under constant stirring and the pH value was adjusted to around 7. After 30 min, 50 mL of 1 mM $AuCl_4^-{}_{(aq)}$ solution was added, and the reaction allowed proceeding for 12 h under consisting stirring. After the reaction, the resultant products were centrifuged, thoroughly washed with deionized water and ethanol, and dried at 60 ºC. Corresponding to an adjustable Au/(Zn_2SnO_4/SnO_2) mass ratio of 0.5%, 1%, 2%, 3% and 4% according to the initial amount of raw materials, the prepared Au nanoparticles inlaid of Zn_2SnO_4/SnO_2composites are denoted as AZS0, AZS1, AZS2, AZS3 and AZS4 samples, respectively.

2.2 Solar cell fabrication

Preparation of Au nanoparticles inlaid Zn_2SnO_4/SnO_2 hollow rounded cubes photoanodes

To prepare the photoanodes of Au nanoparticles inlaid Zn_2SnO_4/SnO_2 hollow rounded cubes, Fluorine doped tin oxide (FTO) glass as transparent conducting glass was cleaned by sonication in soapy water, acetone and ethanol for 20 min respectively. Firstly, the blocking layer solution was created by treating with an aqueous solution of $TiCl_4$(40 mM) at 60 ºC for 15 min to restrain interfacial recombination of electrons in the highly conducting FTO and the I^{3-} oxidized electrolyte.[56] Secondly, a layer of photoanodepaste was spin-coated onto the FTO glass plates by the spin coating method at a speed of 2000 rpm for 30 seconds. The thickness of the photoanode is about 10 mm obtained by repetitive spinning several times.[57]

Fabrication of DSSCs

The annealed electrodes were sensitized by immersing into a 5×10^{-4} MN719 (*cis*-diisothocyanato-bis(2,2'-b -ipyridyl-4,4'-dicarboxylato) ruthenium($_{II}$) bis(tetrabutyl-ammonium)) dye solution dissolved in equal volumes of acetonitrile (Aladdin-reagent, China) and *tert*-butanol (Aladdin- reagent, China) at ambient temperature for 24 h, followed by washing with acetonitrile to remove non-chemisorbed dye, and dried before being assembled in solar cells. The Pt counter electrodes were prepared by coating with a drop of 0.01 M H_2PtCl_6ethanol solution on the cleaned FTO glass and sintered at 400 ºC for 15 min. The two electrodes were thermally sealed together with a 25 μm thick Surlyn polymer seal (Surlyn, DuPont) into a sandwich type cell. The electrolyte

(electrolyte of 0.6 M 1-methy-3-propylimidazolium iodide (PMII), 0.05 M LiI, 0.05 M I_2 and 0.5 M 4-tert-butylpyridine (TBP) in a (85: 15 vol%) mixture of acetonitrile (Aladdin-reagent, China) and valeronitrile (Aladdin-reagent, China)) were injected through a hole in the counter electrode of the assembled cell and driven into the cell via vacuum backfilling. The hole was sealed using another piece of slide glass-backed Surlyn.

2.3 Characterization

The composition and crystal structure of the obtained nanocrystals were examined with an X-ray diffractometer (Philips Rigaku D/Max-kA X-ray diffractometer equipped with a Cu Ka source at 40 kV and 30 mA). The surface morphology of the as-prepared samples was analyzed by SU-70 field-emission scanning electron microscopy (FESEM). The detailed microstructure of the synthesized product was analyzed by using a Phillips Tecnai 20U-Twin high-resolution transmission electron microscope attached to an X-ray energy dispersive spectrometer (EDS) at an acceleration voltage of 200 kV. The surface area of the samples was evaluated by the Brunauer–Emmett–Teller (BET) method using $N2$ physisorption analysis at 77 K with a Gold APP V-Sorb 2800P. Porosity distributions were calculated from the adsorption branch of the isotherm using the corrected form of the Kelvin equation by means of the Barrette–Joynere–Halenda (BJH) method. Prior to physisorption, the samples were degassed at 160 ^{o}C under vacuum for 3 h.

Diffused reflection spectra were measured on a TU-1901 spectro-photometer with an integating sphere detector. The photoluminescence (PL) spectra were recorded using a conventional spectrometer (Cary-50 Varian Co.). Current–voltage characteristics under simulated AM 1.5 illumination were measured using a solar simulator (Newport, Class 3A, 94023A) at one sun (AM 1.5G, 100 mW cm^{-2}) by using a Keithley 2420 source meter equipped, and light intensity was measured using a calibrated Si solar cell (certificated by NREL). The photoactive area of 0.16 cm^{2}was defined by a black metal mask slightly larger than the active area to cut off stray light.[58] The electrochemical impedance spectroscopy (EIS) measurements were performed using a Princeton Parstate 2273A in a two-electrode design; the photoanode served as a working electrode and the Pt-coated on FTO as a counter electrode at an applied bias of the open circuit voltage under one-sun irradiation. The frequency range of 100 mHz to 100 kHz with an AC voltage magnitude of 10 mV. The EIS data were analyzed with an appropriate equivalent circuit using simulation software.

3. Results and discussion

3.1 Structure and morphology characterization

Fig. 1 shows the X-ray diffraction (XRD) patterns of pure Zn_2SnO_4/SnO_2 (a)and Au-Zn_2SnO_4/SnO_2 with different Au loadings: (b) 0.5 wt%, (c) 1 wt% , (d) 2wt% (e) 3w% and (f) 4w%. From the XRD patterns of pure $Zn_2SnO_4/SnO_2$and Au-Zn_2SnO_4/SnO_2, the peaks located at 17.7°, 29.2°, 34.3°, 41.7°, 55.1° and 60.5° can be observed distinctly in all patterns, in good agreement with (111), (220), (311), (400), (511) and (440) planes of inverse-spinalZn_2SnO_4 (JCPDS.24-1470), respectively. The peaks at of 26.4°, 33.7°, 51.6°, correspond well to (110), (101) and (211) planes of tetragonal retile SnO_2 (JCPDS. 41-1445),respectively. Compared with XRD pattern of pure Zn_2SnO_4/SnO_2samples, three additional peaks in XRD pattern of Au-Zn_2SnO_4/SnO_2 are observed at 38.1°, 44.4°, 64.5°(Fig. 1b, c and d), corresponding well to (111), (200), (220) planes of cubic Au, respectively (JCPDS.04-0784). Furthermore, with increasing of the loading amount of Au (from 0.5 w% to 4 w%), the intensity of diffraction peaks at 38.1°, 44.4°, 64.5° increases gradually (Fig. 1b-d).

For the growth of Zn_2SnO_4/SnO_2 hollow rounded cubes, it is found that the concentration of NaOH plays an essential role on the morphologies of precursor $ZnSn(OH)_6$. Fig. S1 displays the SEM images of precursor $ZnSn(OH)_6$ prepared under different concentrations of NaOH. As the amount of NaOH is 60 mmol, the morphology of obtained precursor $ZnSn(OH)_6$ is cube-liked and uniform (Fig. S1a). The high SEM image in Fig.S1b reveals a well-defined cube-shaped structure with a side length of 0.7 μm. With the increasing of the concentration of NaOH, the morphology of $ZnSn(OH)_6$ evolves into rounded cube and the length of sides increases to 1.2μm (Fig. S1d and S1f). When the amount of NaOH increases to 78 mmol, it can be seen from Fig. S1g and 1f that the products becomes uniform qusi-spheres with a diameter of 1.5 μm.

Fig. 2 depicts SEM images of pure Zn_2SnO_4/SnO_2 hollow rounded cubes annealed at 800^{o}C (ZS) and Zn_2SnO_4/SnO_2 hollow rounded cubes inlaid by 2% Au nanoparticle (AZS2). From the SEM images of Fig. 2a-2b, it can be clearly seen that the obtained Zn_2SnO_4/SnO_2 samples are composed of uniform rounded cubes with a side length of 1.2μm. Moreover, the high-resolution SEM images in Fig. 2b suggest that the structure of prepared rounded cubes is hollow nature. After loading of Au nanoparticles (Fig. 2c-2d), both the Zn_2SnO_4/SnO_2hollow rounded cube shape and monodisperse size distribution are maintained, and deposition of Au nanoparticles on surface of Zn_2SnO_4/SnO_2 is uniform (no significant aggregation at the surface is detected). Fig. S2 is the cross-section image of photoanode of Zn_2SnO_4/SnO_2 after absorbing dye N719. The thickness of photoanode film shown in Fig. S2 is around 12 μm.

The microstructure of Au inlaid Zn_2SnO_4/SnO_2hollow rounded cubes (AZS2) are further investigated by TEM. Fig. 3a-3c depict low- and high-magnification TEM images of the AZS2, confirming the hollow rounded cubes are composed of nanoparticles with a size of about 40 nm, and are highly porous. In addition, the high-magnification TEM image in Fig. 3c further demonstrates that Au nanoparticles disperse uniformly on the surface of Zn_2SnO_4/SnO_2.The HRTEM lattice image in Fig. 3d suggests that the coexistence of three kinds of phases of $Zn_2SnO_{4,}$ $SnO_2$and Au. Fig. 3e depicts the HRTEM lattice image of Au nanoparticles, suggesting that the diameter of Au nanoparticle is estimated to be around 10 nm , and two sets of lattice spacing of 0.23 nm and 0.20 nm correspond well with d-spacing of (111) and (200) planes of cubic Au, respectively (JCPDS.04-0784). The electron diffraction (ED) pattern reveals the phase components of the AZS2 samples (Fig. 3f), the diffraction rings correspond well to that of (111), (220) and (400) planes of inverse-spinel Zn_2SnO_4, and (110), (101) and (211) planes of tetragonal rutile SnO_2, respectively. While the diffraction ring of (111) plane of cubic Au is also depicted in Fig.3f.

In order to further investigate the distribution information of Au nanoparticles, energy dispersive X-ray spectroscopy (EDS) elemental mapping analysis is performed on the AZS2 samples. The EDS elemental mapping images in Fig. 4 show the presence of O, Zn, Sn and Au elements distribute throughout the sample, demonstrating the coverage of Au nanoparticles over the entire surface of Zn_2SnO_4/SnO_2. It is worth mentioning that the dispersion of Au nanoparticles is uniform, and no aggregation of Au nanoparticles is observed in Fig. 4d.

The nitrogen absorption-desorption isotherms depicted in Fig. 5are utilized to characterize the textural properties of specific surface area, pore size distribution and pore volume of pure Zn_2SnO_4/SnO_2 hollow rounded cubes (ZS) and Zn_2SnO_4/SnO_2 hollow rounded cubes inlaid with various contents of Au nanoparticles (AZS0, AZS1 ,AZS2, AZS3 and AZS4). As shown in Fig. 5a, all samples display the isotherm with a smooth capillarycondensation step occurred at a relative pressure of ($P/P_0 \approx$ 0.9-1.0) and H3 type hysteresis loops, indicating their relatively large pore size and large specific surface area. An estimate of the mean pore size can be obtained from $4V/A$, where V is the total pore volume and A is the specific area. The mean size of pure Zn_2SnO_4/SnO_2(ZS) and Au inlaid Zn_2SnO_4/SnO_2 (AZS0, AZS1, AZS2, AZS3 and AZS4) are around 30 nm. Textural properties including surface area, pore size and pore volume of all samples are listed in Table 1. With an increase in Au depositing content, the surface area increase slightly from 11.59 $m^2\ g^{-1}$ for ZS to 21.24 $m^2\ g^{-1}$ for AZS4, and the pore size and pore volume decrease from 38.33 nm and 0.377 $cm^3\ g^{-1}$ for ZS to 24.4 nm and 0.113 $cm^3\ g^{-1}$ for AZS2 owing to the Au nanoparticles deposited on the surface and interior of Zn_2SnO_4/SnO_2hollow structure. It is generally accepted that the UV absorption and electron mobility are related to the specific area. A large specific surface area can facilitate electron transfer and provide a sufficient absorption amount of dye molecules, which results in enhanced photovoltaic performance.[59,60]

Table 1 Structural properties of Zn_2SnO_4/SnO_2 and Au-Zn_2SnO_4/SnO_2hollow rounded cubes

Samples	Surface area / $m^2\ g^{-1}$	Pore size / nm	Pore volume / $cm^3\ g^{-1}$
ZS	11.59	38.33	0.377
AZS0	12.66	33.31	0.259
AZS1	15.03	37.72	0.321
AZS2	18.48	24.24	0.113
AZS3	19.21	20.83	0.173
AZS4	21.24	21.66	0.214

3.2 Optical property characterization

Fig. 6shows the UV-vis diffusion reflection spectra (DRS) of pure Zn_2SnO_4/SnO_2 (ZS) and Au inlaid Zn_2SnO_4/SnO_2 (AZS0, AZS1, AZS2, AZS3 and AZS4). The DRS of pure Zn_2SnO_4/SnO_2(ZS) shows a strong diffusion reflection of light over 400-700 nm and drops suddenly in the range of 300-400 nm, indicting the Zn_2SnO_4/SnO_2 composite displays a wide-band-gap and nearly no absorption in the range of visible light. After inlaid with different contents of Au nanoparticles, the diffusion reflection spectra decrease significantly compared with that of ZS and show an obvious sunken at about 550 nm, in goodcorrespondence with the LSPR characterization of Au nanoparticles.[61] The evolution of diffusion reflection spectra can be attributed to inducement of LSPR effect of Au nanoparticle to the absorption in visible light. Moreover, with the increasing of Au content, the LSPR effect is more enhanced, as shown in Fig. 6 (AZS0, AZS1 and AZS2). Whereas, the UV-vis diffusion reflection for AZS3 and AZS4 does not increase compared with AZS2, indicating that the

LSPR effect as reached its limit. The UV-vis diffusion reflection spectra confirm that Au nanoparticles play a significant role to enhance the visible light absorption for wide-band-gap semiconductor material of Zn_2SnO_4/SnO_2. The surface plasmonic resonance induced by Au nanoparticles can cause strong local field enhancement around Au nanoparticles, which can increase the light absorption of the surrounding dyemolecules in a dye-loaded film. Therefore, enhancement of the light harvesting efficiency and hence the photocurrent of a DSSC can be expected using such Au–Zn_2SnO_4/SnO_2photoanode.

Photoluminescence (PL) emission spectra are used to investigate the effect of the Au nanoparticles on the properties of charge carrier trapping, immigration and transfer, as well as to understand the fate of photo-generated electron-hole pairs in the Au laid Zn_2SnO_4/SnO_2 composite. Fig. 7 shows the PL emission spectra of pure Zn_2SnO_4/SnO_2 (ZS) and Au inlaid Zn_2SnO_4/SnO_2 (AZS0, AZS1, AZS2, AZS3 and AZS4) at room temperature. The PL emission spectrum for ZS, AZS0, AZS1, AZS2, AZS3 and AZS4 are obtained by using a spectrophotometer containing a xenon lamp with 350 nm excitation wavelengths. The energy of the excitation light is enough to promote electronic transition from the valence band to the conducting band of these four samples according to the above DRS (Fig. 6). All samples show two characteristic emission peaks at around 470 nm and 560 nm in the PL emission. The band-gaps of Zn_2SnO_4 and SnO_2 are all 3.6 eV. Because of the limit of the PL detection range, the band-to-band emission peak (≈340 nm) of the $Zn_2SnO_4$and $SnO_2$is not observed. For the PL mechanism of Zn_2SnO_4 and SnO_2, it is considered to be attributed to other luminescence centers, such as oxygen deficiency and surface states during the growth process. Su et al.[62] reported the optical properties of single-crystalline Zn_2SnO_4 nanowires synthesized by thermal evaporation route, demonstrating that PL of the nanowires display a strong green emission band at 580 nm.Wang's.[63] study suggests that Zn_2SnO_4 nanobelts show a broad blue-green PL emission around 400–600 nm with a maximum at 490 nm. In the present work, the peaks at 470 nm and 560 nm may be contributed to the oxygen deficiency of Zn_2SnO_4 and SnO_2.

For AZS0, AZS1, AZS2 and AZS3 in Fig. 7, the decrease of PL intensity of the emission peaks indicate that the presence of Au can suppress the recombination rate of electron-hole pairs.[52] In addition, the intensity of emission peak depends on the concentration of Au. 0.5w% Au inlaid Zn_2SnO_4/SnO_2 (AZS0) shows a similar PL peak with pure Zn_2SnO_4/SnO_2, indicating that the effect of contents of trace Au to inhibit recombination of photo-induced electron-hole pairs is not significant. However, with the increasing of amount of Au to 1w% (AZS1), the intensity of emission peak decreases markedly compared with that of ZS and AZS0, demonstrating that Au nanoparticles play a key role to suppress the recombination rate of photo-induced electron-hole pairs. As the concentration of Au is up to 4%, the PL peak increases sharply. The high Au content (4w%) may inhibit recombination to a certain extent, this is because a high Au incorporation may create some new electron-hole pairs recombination centers, which could counteract its positive effect on the restraint of the recombination of electron-hole pairs.

The mechanism of Au nanoparticle to inhibit recombination rate of photo-induced electron-hole pairs can be illustrated by energy band-gap model of Scheme 1. Owing to the flowing of electrons from Zn_2SnO_4/SnO_2composite to Au nanoparticles, negative charge at the surface of Au and positive charge on the surface of semiconductor both increase, which causes the space charge region formation at interface between Au nanoparticles and Zn_2SnO_4/SnO_2composite. Therefore, electric field emerges in the space charge region, making the energy band bend, and ultimately, surface a potential of V_s generate between the surface and interior of Zn_2SnO_4/SnO_2. The barrier height in semiconductor can be expressed as:

$$qV_D = -qV_s = W_m - W_s \tag{1}$$

and the barrier height in Au can be expressed as:

$$q\phi_{ns} = qV_D + E_n = -qV_s + E_n = W_m - W_s \tag{2}$$

in which V_s is surface potential between the surface and interior of Zn_2SnO_4/SnO_2, W_m is the work function of metal defined as the difference between the Fermi level and vacuum level, W_s is the work function of semiconductor, and E_n is the difference between the Fermi level and bottom of conduction band for semiconductor. When an electron excited from Zn_2SnO_4/SnO_2composite, it is unlikely to go back due to the presence of this barrier.

3.3 The performance of solar cells

3.3.1 Photocurrent-voltage (J-V) curves analysis

The photocurrent density (J)-voltage (V) characteristics of DSSCs based on N719 sensitized pure $Zn_2SnO_4/SnO_2$and Au-$Zn_2SnO_4/SnO_2$with different Au loading contents are measured under AM 1.5G illumination (100 mW cm^{-2}). Fig. 8 shows the J-V curves for each single DSSCs and the corresponding photovoltaic parameters are summarized in Table 2, indicating that the incorporation of Au nanoparticles plays a significant role on the photovoltaic performance of DSSCs. For DSSCs based on Zn_2SnO_4/SnO_2, the open-circuit voltage is 674 mV and short-circuit photocurrent density is 2.64 mA cm^{-2}. The power conversion efficiency measured is 1.18%. After loading with Au nanoparticles, V_{oc} depicts an obvious decrease to 587 mV. While J_{sc} shows a significant increase to 4.04 mA cm^{-2}. With the increasing of the Au incorporation content ranging from 0.5% to 2%, the short-circuit photocurrent of Au-Zn_2SnO_4/SnO_2increase from 4.04 mA cm^{-2} (Au 0.5%) to 5.88 mA cm^{-2} (Au 2%). Similarly, V_{oc} always keeps increasing trend and is measured to be 600 mV as the Au content reaches 2%. Fill Factor (FF) shows a slight decline trend with the increasing of Au concentration except for AZS1. It is worth noting that the dye concentration is 34.41 nmol cm^{-2} for ZS, and display a slight increase to 43.23 for AZS2, which indicting that increased surface area of $Zn_2SnO_4/SnO_2$is a direct consequence of enhanced dye loading capacity. The eventual photovoltaic conversion efficiency reaches 2.04% for 2% Au inlaid Zn_2SnO_4/SnO_2, showing enhancement of power conversion efficiency by 73%. However, with increasing Au concentration to 4%, the current density and photovoltaic conversion efficiency display a slightly decrease (5.29 mA cm^{-2} and 1.85%). This may be attributed to more electron-hole pairs recombination centers caused by increasing Au content, which could counteract its positive effect on the restraint of the recombination of electron-hole pairs.

Table 2 Performance of DSSCs based on ZS, AZS0, AZS1 and AZS2samples under AM 1.5 simulation illumination

Samples	V_{oc} (mV)	J_{sc} (mA cm^{-2})	Fill Factor (%)	η^a (%)	Dye adsorption (nmol cm^{-2})
ZS	674	2.64	66.3	1.18	34.41
AZS0	587	4.04	58.6	1.39	36.21
AZS1	594	4.98	60.2	1.69	39.74
AZS2	600	5.88	57.7	2.04	43.23
AZS3	607	5.62	58.2	1.99	44.67
AZS4	616	5.29	57.1	1.85	45.21

η^a(%) = $J_{sc}V_{oc}FF/P_{in}$, where P_{in} = 100mW cm^{-2}(AM 1.5). Each η is an average value obtained from four samples.

3.3.2 Incident photo-to-electron conversion efficiency (IPCE)

The corresponding incident monochromatic photon-to-electron conversion efficiency (IPCE) spectra are shown in Fig. 9. IPCE is defined as the number of generated electrons divided by the number of incident photons. The IPCE spectra indicate that the maximum efficiency is obtained at a wavelength of around 520 nm, in coincidence with the absorption wavelength of the N719 dyes and Au nanoparticles. Clearly, with the incorporation content of Au nanoparticles increasing from 0.5w% to 2w%, the intensity of IPCE increases, displaying s similar trend to that of J_{sc}. Analogous tendency can also been seen for DSSCs based 3% and 4% Au concentration. As the content of Au is 2%, it reaches a maximum IPCE of ~50% for AZS2 sample. An obvious of IPCE feature is the spectrum broadening to a longer wavelength with the increase amount of Au nanoparticles inlaid on Zn_2SnO_4/SnO_2, attributing to the effect of the plasma resonance effect.

3.3.3 Electrochemical impedance spectroscopy (EIS) spectra analysis

Electrochemical impedance spectroscopy (EIS) measurements are performed to investigate the interfacial reaction of photoexecited electrons and the electron transport kinetics of DSSCs based on $Zn_2SnO_4/SnO_2$and Au inlaid Zn_2SnO_4/SnO_2. Fig. 10a depicts the Nyquist plots of DSSCs based on ZS, AZS0, AZS1, AZS2, AZS3 and AZS4 film electrodes. The equivalent circuit is shown as the inset in Fig. 10a using non-linear-least-square (NLLS) fit analysis software (Zview software) and the fitting data are given in Table 3. R_s can be recognized and fitted according to an equivalent circuit model as the resistance of the interface of FTO and photoelectrode material. The R_s value of DSSCs based on ZS, AZS0, AZS1, AZS2, AZS3 and AZS4 calculated according to the equivalent circuit is 6.04, 4.03, 7.28, 3.66, 6.21 and 2.65 Ù, respectively. It is clearly that the value of R_s for AZS0 and AZS2 is better than that of ZS and AZS1 counterparts, implying better electronic contact at the interface between FTO and photoelectrode for AZS0 and AZS2. The big semicircle in the Nyquist plot corresponds to the electron transfer resistance at the oxide/dye/electrolyte interface, larger resistance is observed for Zn_2SnO_4/SnO_2(312.6 Ù) compared to Au inlaid Zn_2SnO_4/SnO_2(275.6 Ù). Moreover, with the concentration of Au increasing, the resistance at the interface decreases from 275.6 Ù to 147.8 Ù, demonstrating the less electron transport resistance and less electrons going back to the electrolyte at the oxide/electrolyte interface.[64] It is known that the noble metal nanoparticles can cause a potential barrier at the surface of oxide semiconductor, preventing the recombination of electron-holes (Fig. 10b). This result comes to the same conclusion as PL spectra. However, for 4% Au inlaid Zn_2SnO_4/SnO_2, its electrochemical impedance in intermediate-frequency region is larger than 3% Au inlaid Zn_2SnO_4/SnO_2.

In order to further demonstrate Au inlaid in Zn_2SnO_4/SnO_2 can reduce recombination rate of photogenerated electron-hole pairs, the impedance spectra of pure Zn_2SnO_4/SnO_2 and Au inlaid Zn_2SnO_4/SnO_2 are measured under forward bias in the dark (Fig. 3S). Responses in the intermediate-frequency region are assigned to charge-transfer processes occurring TiO_2/dye/electrolyteinterface.[65] In the dark, the DSSC behaves as a leaking capacitor.[66] Under forward bias in the dark, electrons are transported through the TiO_2 network and react with I_3^-. At the same time, I^- is oxidized to I_3^- at the counter electrode. The dark reaction impedance due to electron transfer from the conduction band of TiO_2 to triiodide ions in the electrolyte is presented by the semicircle in intermediate-frequency regime in the Nyquist plots. The bigger the middle frequency semicircle in the Nyquist plots is, the smaller the recombination rate for electron at the TiO_2/dye/electrolyte interface is. Strikingly, the impedance due to electron transfer from the conduction band of photoelectrode film to triiodide ions in the electrolyte, presented by the semicircle in the intermediate-frequency regime, shows a gradually increasing tendency with the Au content increase, meaning the recombination rate of photogenerated electron-hole pairs diminishes.

Bode phase plots of EIS can offer the lifetime information of electrons during the photovotaic process,as shown in Fig. 10b. According to EIS model developed by Kern et al,[67] the lifetime of electrons on the photoanodes (τ) can be calculated according to the relation $\tau = 1/\omega_{max} = 1/(2\pi f_{max})$, where f_{max} is the maximum frequency of the medium-frequency peak. The f_{max} located at 63.19 Hz for Zn_2SnO_4/SnO_2(ZS) is much smaller than 102.23 Hz for 2% Au inlaid Zn_2SnO_4/SnO_2(AZS2), suggesting τ in the ZS (2.70 ms) film is longer than that for AZS2 (1.56 ms). While the τ for AZS1 is longer than any other samples. This may be attributed to the effects of two aspects together. On the one side, the enhancement of Au loading can cause the potential barrier on the surface of Zn_2SnO_4/SnO_2, which can suppress the recombination of electrons and holes. On the other side, increasing the amount of Au nanoparticles may introduce more traps for electrons, counteracting its positive effect on the restraint of the recombination of electron-hole pairs.

Table 3 Resistances and electron lifetime of DSSCs based on different photoanodes

Samples	R_s (Ù)	R_p (Ù)	Frequency (Hz)	T (ms)
ZS	6.04	312.6	63.19	2.70
AZS0	4.03	275.6	99.23	1.60
AZS1	7.28	204.6	55.11	2.89
AZS2	3.66	181.2	102.23	1.56
AZS3	6.21	147.8	143.21	1.11
ASZ4	2.65	193.3	145.14	1.10

3.3.3 DSSCs configuration and related mechanism

In order to better understand the reasons for the performance variation of DSSCs including open-circuit voltage, short-circuit photocurrent density, Fill Factor and power conversion efficiency, the DSSCs construction

(Fig. 11) is depicted and the related mechanism is investigated. The proposed charge transfer process in oxide/Au/dye/electrolyte is illustrated in Fig. 11. Zn_2SnO_4 and SnO_2 are both wide band-gap semiconductors with same band-gap of 3.6 eV. Both valence band and conduction band of $Zn_2SnO_4$are more negative than that of the SnO_2 counterpart.[37] The good match of band edges between Zn_2SnO_4 and SnO_2 is important to form a type Ⅱ heterojunction. In addition, the LOMO of dye is more negative than the conduction band edge of oxide, which is an essential condition for the normal state of DSSCs. Under UV irradiation, electrons photogenerated from the dye pass through the Au nanoparticles, along the lower lying conduction band of Zn_2SnO_4 to the lowest conduction band edge of SnO_2, while the photogenerated holes in dye are reduced by I^- in electrolyte. Furthermore, the surface plasmatic resonance created by Au nanoparticles can cause strong local field enhancement around Au nanoparticles, which can increase the lightabsorption of the surrounding dye molecules in a dye-loaded film and boost the photogenerated electrons consequently. Besides the spatial separation of charge carrier acceleration caused by simultaneous transfer of electrons and holes in Zn_2SnO_4/SnO_2/Au/dye system, it is worth noting that a barrier formed on the surface of oxide semiconductor due to the effect of Au nanoparticles as elaborated before, which reduces the probability of recombination of electrons and holes.

Two elucidations can be accounted for the enhancement of the short-circuit photocurrent density. The localized surface plasmon resonance (LSPR) of Au nanoparticles, on the one hand, plays a key role to the enhancement of the short-circuit photocurrent density. The increase can be attributed to the boost of visible light absorption (Fig. 6). By proper coupling with of Au nanoparticle onto Zn_2SnO_4/SnO_2, light can be efficiently trapped and concentrated by dyes, as a result of which, the optical absorption and photocurrent can be enhanced significantly. On the other hand, the decrease of electron-hole recombination rate is essential to improvement of photocurrent density, which can be attributed to three primary reasons. First and foremost, potential barrier on the surface of oxide semiconductor caused by Au nanoparticles hinders the recombination of electrons and holes. When an electron passes along the conduction band edge of Zn_2SnO_4/SnO_2composite, it is unlikely to go back to the dye or electrolyte due to the presence of this barrier. Second, the compositing of Zn_2SnO_4 and SnO_2 to form heterojunction can suppress recombination of electrons and holes, which increases the separation efficiency of photo-induced electron-hole pairs in surface and interface. Third, it is the close contact among rounded cubes and hollow structure that increases the electron mobility, and reduces the probability of recombination.

The evolution of open circuit voltage with the increasing content of Au nanoparticles can be explained as follows. For the Au inlaid Zn_2SnO_4/SnO_2, the open circuit voltage shows a sharply decrease trend compared with Zn_2SnO_4/SnO_2. The reason can be explained as follows. The Fermi level corresponding to Au inlaid Zn_2SnO_4/SnO_2 is created because the electrons in Au nanoparticles and Zn_2SnO_4/SnO_2 are moved to attain a stable balance. The Fermi level of Au nanoparticle is lower than the counterpart of Zn_2SnO_4/SnO_2composite. If such metal particles come in contact with a charged semiconductor nanostructure, the electron in semiconductor will flow to the side of metal nanoparticle, making electrons accumulate on the surface of metal and holes aggregated on the surface of semiconductor. Consequentially, in order to balance the charge between the metal and semiconductor, the Fermi level shifts to more positive compared with Zn_2SnO_4/SnO_2. It is known that the open circuit voltage in electrochemical DSSCs is limited by the difference between the Fermi level of electron-conducting nanostructure and the redox potential of the electrolyte. The open circuit voltage for Au-Zn_2SnO_4/SnO_2, therefore, shows a decrease (587, 596 and 600 mV) compared with Zn_2SnO_4/SnO_2composite (674 mV). However, it is interesting to note that with the increasing of loading amount of Au, the open circuit displays a slight increase. This is because the Fermi level of Zn_2SnO_4/SnO_2 semiconductor dictates the energetic of the reduction process at the semiconductor-dye interface. The Fermi level of an n-type semiconductor is determined by expression 3[68]

$$E_F = E_c + kT \ln \frac{n_c}{N_c} \tag{3}$$

Where E_c is the conduction-band energy level, n_c is the density of net ionized states (or accumulated electrons in the present case), and N_c is the density of state at the conduction band. The position of the Fermi level that lies between the valance and conduction bands is dependent on the electron accumulation within the semiconductor particles. As more electrons are accumulated within the CB of Zn_2SnO_4/SnO_2, the Fermi level becomes more negative and shifts closer to the conduction band edge of Zn_2SnO_4/SnO_2, as shown in Fig. 11.

On the basis of the above experiment results, the highest power conversion efficiency of the DSSCs based on 2%Au inlaid Zn_2SnO_4/SnO_2 (AZS2) electrode can be attributed to the effect of three factors. Firstly, the localized surface Plasmon resonance (LSPR) of Au nanoparticles plays a crucial role to the enhancement of visible light absorption as shown in Fig. 6, which increases the photocurrent density significantly. Secondly, the potential barrier on the Zn_2SnO_4/SnO_2 surface caused by Au nanoparticles can suppress electron-hole recombination, diminish the loss of electrons during transfer process and improve the photocurrent density, which are demonstrated in PL emission spectra and EIS spectra. Thirdly, the enhanced photovoltaic performance can be also attributed to unique structural characteristics of hollow rounded cubes. It has been shown that hollow rounded cube structured 2%Au–Zn_2SnO_4/SnO_2 sample displays a high surface area (18.48 m^2 g^{-1}) and high dye adsorption (43.23 nmol cm^{-2}). Accordingly, the 2% Au–Zn_2SnO_4/SnO_2 sample possesses higher power conversion efficiency than that of Zn_2SnO_4/SnO_2sampleand therefore exhibits enhanced photovoltaic performance.

4. Conclusions

A facile strategy has been developed for fabrication of Au inlaid Zn_2SnO_4/SnO_2 hollow rounded cubes with an adjustable Au loading content using Inns(OH)$_6$ as precursors, chloroauricacid as Au source and ascorbic acid as reducing agent. The micro/nanostructure and chemical compositions of Zn_2SnO_4/SnO_2 and Au inlaid Zn_2SnO_4/SnO_2samples were characterized using XRD, SEM, TEM, EDS and N_2 adsorption and desorption techniques. The photovoltaic performance was evaluated by DRS, PL, J-V, IPCE and EIS techniques. As photoanodes for DSSCs, the Au-Zn_2SnO_4/SnO_2 hollow rounded cubes demonstrate a greatly enhanced J_{sc} and improved power conversion efficiency of up to 2.04%, which increase by 73% relative to that of Zn_2SnO_4/SnO_2 based DSSCs. The relation of microstructure, optical response, electron transfer and photovoltaic performance is discussed and analyzed. The enhancement of photovoltaic performance of Au inlaidZn_2SnO_4/SnO_2 hollow rounded cubes can be attributed to the following reasons. The well-distributed Au nanoparticles boost the light absorption significantly due to the effect of localized surface plasmon resonance (LSPR) and suppress the recombination rate of electron-hole pairs via forming potential barrier on the surface of Zn_2SnO_4/SnO_2. In addition, the high crystalline state, large surface area, and large pore size of Au-Zn_2SnO_4/SnO_2 also contribute to the improvement of photovoltaic performance.

Acknowledgments

We acknowledge support from the project supported by the Sate Key Program of National Natural Science of China (No.: 51532005), National Nature Science Foundation of China (No.: 51472148, 51272137), the Tai Shan Scholar Foundation of Shandong Province.

References

1 B. O’Regan and M. Gratzel, *Nature*, 1991, 353, 737-740.

2 M. Law, L. E. Greene, J. C. Johnson, R. Saykally and P. Yang,*Nat. Mater.*, 2005, 4, 455–459.

3 M. D. Brown, T. Suteewong, R. S. Kumar, V. D'Innocenzo, A. Petrozza, M. M. Lee, U. Wiesner and H. J. Snaith, *Nano. Lett.*, 2011, 11, 438–445.

4 Y. H. Jang, X. Xin, M. Byun, Y. J. Jang, Z. Lin and D. H. Kim,*NanoLett.*, 2011, 12, 479–485.

5 W.Q.Wu,Y.F.Xu,H.S.Rao,H.L.Feng,C.Y.Suand, D. B. Kuang, *Angew. Chem., Int. Ed*, 2014, 53, 4816–4821.

6 M. K. Wang, N. Chamberland, L. Breau, J. E. Moser, R. Humphry-Baker, B. Marsan, S. M. Zakeeruddin and M. Gratzel, *Nat. Chem.*, 2010, 2, 385–389.

7 A.Yella,H. W. Lee, H. N.Tsao, C. Yi and A. K. Chandiran,*Science*, 2011, 334, 629-634.

8 H. Wang, X. Zhang, F. Gong, G. Zhou and Z. S. Wang, *Adv. Mater.*, 2012, 24, 121–124.

9 T. Bessho, E. Yoneda, J.H. Yum, M. Guglielmi, I. Tavernelli, H. Imai, U. Rothlisberger, M. K. Nazeeruddin and M. Grätzel, *J. Am. Chem. Soc.*, 2009, 131, 5930–5934.

10 P. G. Bomben, K. C. Robson, P. A. Sedach and C. P. Berlinguette, *Inorg. Chem.*, 2009, 48, 9631–9643.

11 P. G. Johansson, J. G. Rowley, A. Taheri, G. J. Meyer, S. P. Singh, A. Islam and L. Han, *Langmuir*, 2011, 27, 14522–14531.

12 S.Mathew, A.Yella, P.Gao, R Humphry-Baker,F. E. Curchod, N. A. Astani, I. Tavernelli, U. Rothlisberger, M. K. Nazeeruddin and M. Gratzel, *Nat. chem.*, 2014, 6, 242-247.

13 Q. F. Zhang, C. S. Dandeneau, X. Y. Zhou, and G. Z. Cao,*Adv. Mater.*, 2009, 21, 4087–4108.

14 S. H.Ko, D.Lee, H. W. Kang, K. H. Nam, J. Y. Yeo, S. J. Hong,*Nano letters*., 2011, 11, 666-671.

15 S.Gubbala, V.ChakrapaniandV.Kumar, *Adv.Funct. Mater.*, 2008, 18, 2411-2418.

16 H. J. Snaith and C. Ducati, *Nano.Lett.*, 2010, 10, 1259–1265.

17 M. Muruganandham and M. Swaminathan,*Sol. Energy Mater. Sol. Cells*, 2004, 81, 439-457.

18 G. A. Epling and C. Lin, *Chemosphere*, 2002, 46, 561–570.

19 Y. F. Wang, K. N. Li, Y. F. Xu, H. S. Rao, C. Y. Su and D. B. Kuang,*Nanoscale*, 2013, 5,5940–5948.

20 Y. Zhang, H. Zhang, Y. Wang, and W. F. Zhang, *J. Phys. Chem. C*, 2008, 112, 8553–8557.

21 X. Wei, G. Xu, Z. Ren, C. Xu, G. Shen, and G. Han, *J. Am. Ceram. Soc.*, 2008 91, 3795–3799.

22 Q. Dai, J. Chen, L. Lu, J. Tang and W. Wang, *Nano Lett.*, 2012, 12, 4187−4193.

23 L. Bao, J. Zang,G. Wang and X. Li, *Nano Lett.*, 2014, 14, 6505−6509.

24 E. Hendry, M. Koeberg, B. O’Regan and M. Bonn, *Nano Lett.*,2006, 6, 755-759.

25 M. A. Alpuche-Aviles and Y. Wu, *J. AM. CHEM. SOC.*, 2009, 131, 3216–3224

26 B. Tan, E. Toman, Y. Li, and Y. Wu, *J. AM. CHEM. SOC.*, 2007, 129, 4162-4163.

27 Z. Li,Y. Zhou, C. Bao, G. Xue, J. Zhang, J. Liu, T. Yuand Z. Zou,*Nanoscale*, 2012, 4, 3490–3494.

28 Y. F. Wang, K. N. Li, Y. F. Xu, C. Y. Su, D. B. Kuang, *Nano Energy*,2013, 2, 1287–1293.

29 L. Shi and Y. Dai,*J. Mater. Chem. A*, 2013, 1, 12981.

30 L. Huang, L. Jiang and M. Wei, *Electrochem. Commun*., 2010, 12, 319-322

31 Y. Li, X. Zheng, H. Zhang, B. Guo, A. Pang and M. Wei, *Electrochim. Acta.,* 2011,56, 9257-9261

32 Y. Li, A. Pang, X. Zheng and M. Wei, *Electrochim. Acta*, 2011, 56, 4902-4906

33 Y. Li, B. Guo, X. Zheng, A. Pang and M. Wei, *Electrochim. Acta*, 2012, 60, 66-70

34 L. B. Li, Y.F. Wang, H.S. Rao, W.Q. Wu, K.N. Li, C.Y. Suand D.B. Kuang, *ACS Appl. Mater. Interfaces*. 2013, 5, 11865-11871.

35 S. Gubbala, V. Chakrapani, V. Kumar and M. K. Sunkara，*Adv.Funct. Mater.*, 2008, 18, 2411–2418.

36 E. Ramasamy and J. Lee, *J. Phys. Chem. C*, 2010, 114, 22032–22037.

37 Z. Dong, H. Ren, C. M. Hessel, J. Wang, R. Yu,Q. Jin, M. Yang, Z. Hu, Y. Chen, Z. Tang, H. Zhao, and D. Wang, *Adv. Mater.*, 2014, 26, 905–909.

38 B. Li, L. Luo, T. Xiao, X. Hu, L. Lu, J. Wang and Y. Tang, *J. Alloy. Compd*.,2011, 509, 2186–2191

39 C. Liu, R. Roder, L. Zhang,Z. Ren, H. Chen, Z. Zhang, C. Ronning and P. Gao, *J. Mater. Chem. A*, 2014, 2, 4157

40 M. Li, S. K. Cushing, Q. Wang, X. Shi, L. A. Hornak, Z. Hong and N. Wu, *J. Phys. Chem. Lett.*, 2011, 2, 2125–2129.

41 M. D. Brown, T. Suteewong, R. S. Kumar, V. D'Innocenzo, A. Petrozza, M. M. Lee, U. Wiesner,and H. J. Snaith, *Nano Lett.* 2011, 11, 438–445.

42 J. Du,J. Qi, D. Wang and Z. Tang, *Energy Environ. Sci.*, 2012, 5, 6914–6918.

43 S. Chang, Q. Li, X. Xiao, K. Y. Wong and T. Chen, *Energy Environ. Sci.*, 2012, 5, 9444–9448.

44 Y. Li, H. Wang, Q. Feng, G. Zhou and Z. Wang,*Energy Environ. Sci.*, 2013, 6, 2156–2165.

45 J. Qi and X. Dang, *ACS Nano*, 2011, 5, 7108–7116.

46 E. W. McFarland and J. Tang, *Nature*, 2003, 421, 616.

47 G-J.Ke, H-Y. Chen, C-Y. Su and D-B. Kuang, *J. Mater. Chem. A*, 2013, 1, 13274–13282.

48 J. H. Pan, X. Z. Wang, Q. Huang, C. Shen, Z. Y. Koh, Q. Wang, A. Engel, and D. W. Bahnemann, *Adv. Funct. Mater.*, 2014, 24, 95–104.

49 V. Ganapathy,E-H. Kong, Y-C. Park, H. M. Jang and S-W. Rhee,*Nanoscale*, 2014, 6, 3296–3301.

50 S. H. Ahn, D. J. Kim, W. S. Chi, and J. H. Kim, *Adv. Funct. Mater.*, 2014, 24, 5037–5044.

51 Z. Dong, X. Lai, J. E. Halpert, N. Yang, L. Yi, J. Zhai, D. Wang, Z. Tang, and L. Jiang, *Adv. Mater.*, 2012, 24, 1046–1049.

52 C. Yu, K Yang, Y. Xie, Q. Fan, J. C. Yu, Q. Shu and C. Wang, *Nanoscale*, 2013, 5, 2142–2151

53 Z. Y. Wang, D. Y. Luan, C. M. Li, F. B. Su, S. Madhavi,F. Y. C. Boey and X. W. Lou, *J. Am. Chem. Soc.*, 2010, 132,16271–16277.

54 H.Yu, Y. Bai, X. Zong, F. Tang, G. Q. M. Lu and L. Wang,*Chem. Commun.*, 2012, 48, 7386–7388.

55 L. Zhang, H. B. Wu, B. Liu and X. W.Lou, *Energy Environ. Sci.*, 2014, 7, 1013-1017.

56 E. Palomares, J. N. Clifford, S. A. Haque, T. Lutz andJ. R. Durrant, *J. Am. Chem. Soc.*, 2003, 125, 475–482.

57 S. Ito, P. Chen, P. Comte, M. K. Nazeeruddin, P. Liska, P. Pechy and M. Gratzel, *Prog. Photovoltaics*, 2007, 15, 603–612.

58 H. J. Snaith, *Energy Environ. Sci.*, 2012, 5, 6513–6520.

59 S. Yang, D. Yang, J. Kim, J. Hong, H. Kim, I. Kim and H. Lee,*Adv. Mater.*,2008, 20, 1059–1064.

60 J.B.Zhong,D.Ma,X.Y.He,J.Z.LiandY.Q.Chen, *Appl. Surf. Sci.*. 2010, 256, 2859–2862.

61 W. Hou, P. Pavaskar, Z. Liu, J. Theiss, M. Aykol and S. B. Cronin, *Energy Environ. Sci.*, 2011, 4, 4650-4655.

62 Y. Su, L. Zhu, L. Xu, Y. Chen, H. Xiao, Q. Zhou and Y. Feng, *Mater. Lett.*, 2007, 61, 351–354.

63 J.X. Wang, S.S. Xie, H.J. Yuan, X.Q. Yan, D.F. Liu, Y. Gao, Z.P. Zhou, L. Song, L.F. Liu, X.W. Zhao, X.Y. Dou, W.Y. Zhou and G. Wang, *Sol. St. Comm.*2004, 131, 435–440.

64 H. Pang, H. Yang, C. Guo and C. Li, *ACS Appl. Mater. Interfaces*, 2012, 4, 6261−6265.

65 Z. Wang, T. Yamaguchi, H. Sugihara and H. Arakawa, *Langmuir*, 2005, 21, 4272-4276

66 J. Bisquert, *J. Phys. Chem. B.*, 2002, 106, 325-333

67 R. Kern, R. Sastrawan, J. Ferber, R. Stangl and J. Luther, *Electrochim. Acta*, 2002, 47, 4213–4225.

68 M. Jakob and H. Levanon, *Nano Lett.*, 2003, 3, 353-358.

Figure Files

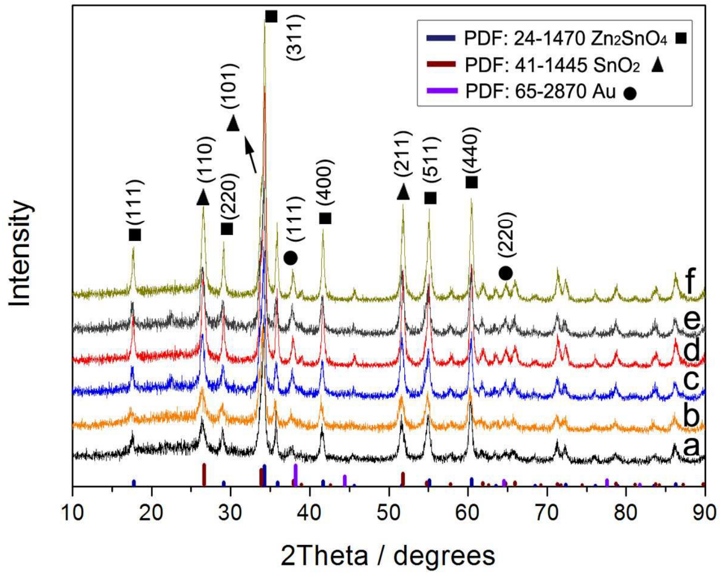

Fig.1 XRD patterns of the as-prepared Zn_2SnO_4/SnO_2 and Au-Zn_2SnO_4/$SnO_2$with different Au/(Zn_2SnO_4/SnO_2) weight ratios: (a) ZS, (b) AZS0, (c) ASZ1, (d) ASZ2.

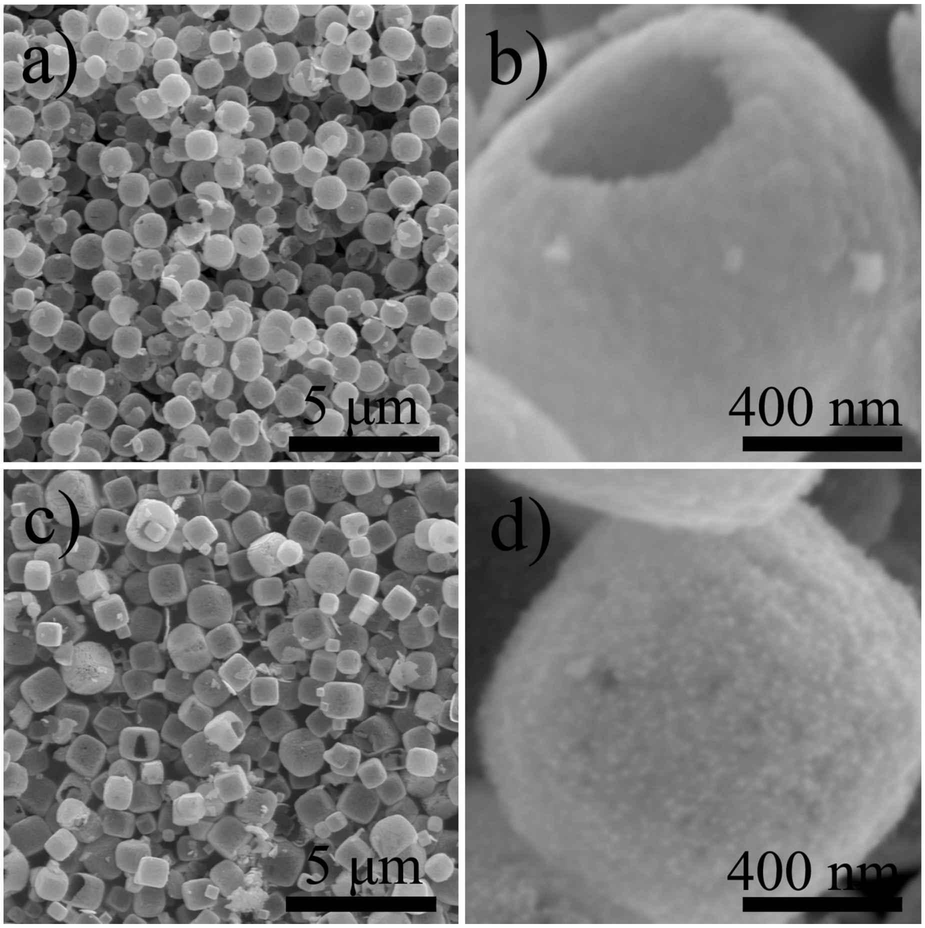

Fig. 2 (a, b) FE-SEM images of as-preparedZn_2SnO_4/SnO_2hollow rounded cubes. (c, d) FE-SEM images of as-prepared 2% Au-Zn_2SnO_4/SnO_2hollow rounded cubes.

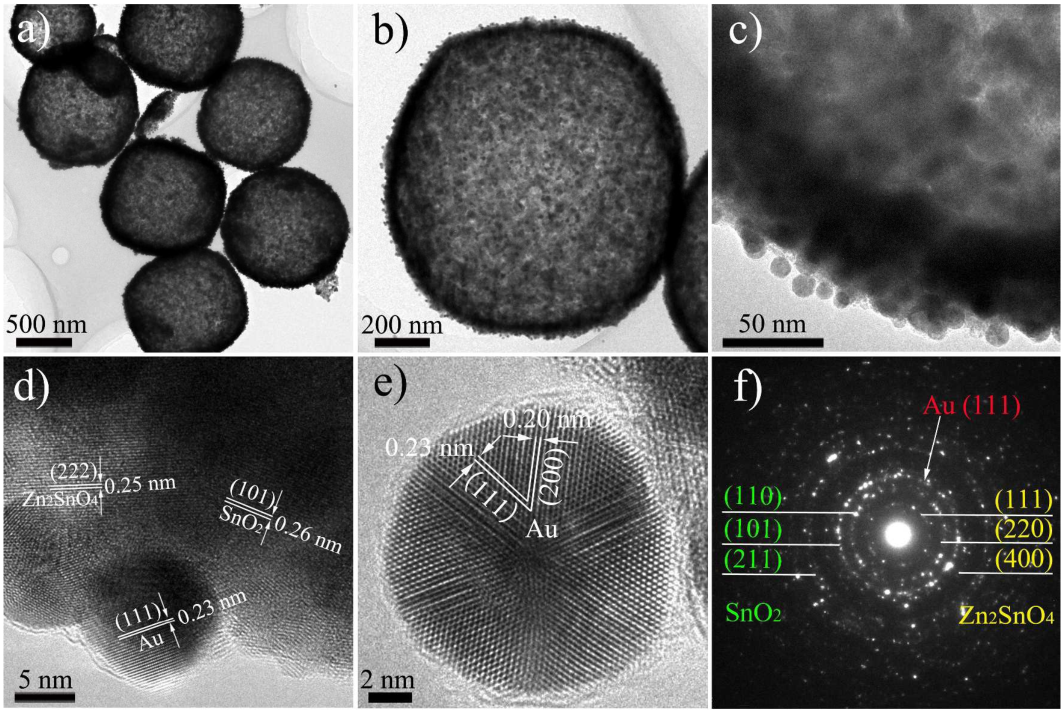

Fig. 3 (a, b) TEM images of AZS2 sample. (c) Magnified TEM images of AZS2 sample. (d, e) HR-TEM lattice images of AZS2 sample. (f) Electrondiffraction pattern of AZS2 sample.

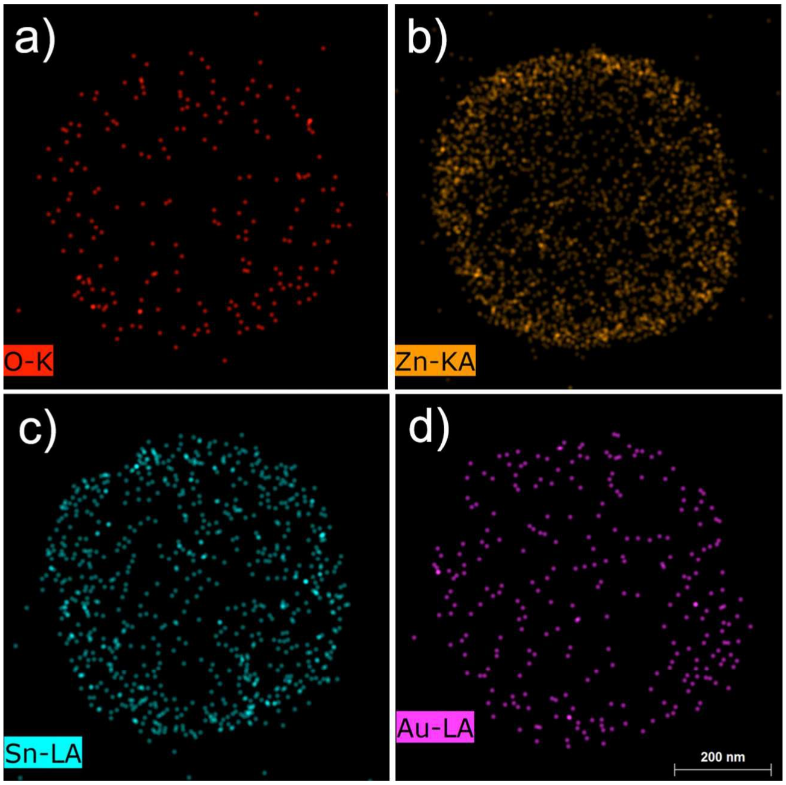

Fig. 4 EDS images for elemental analysis of AZS2 sample: (a) O, (b) Zn, (c) Sn, (d) Au.

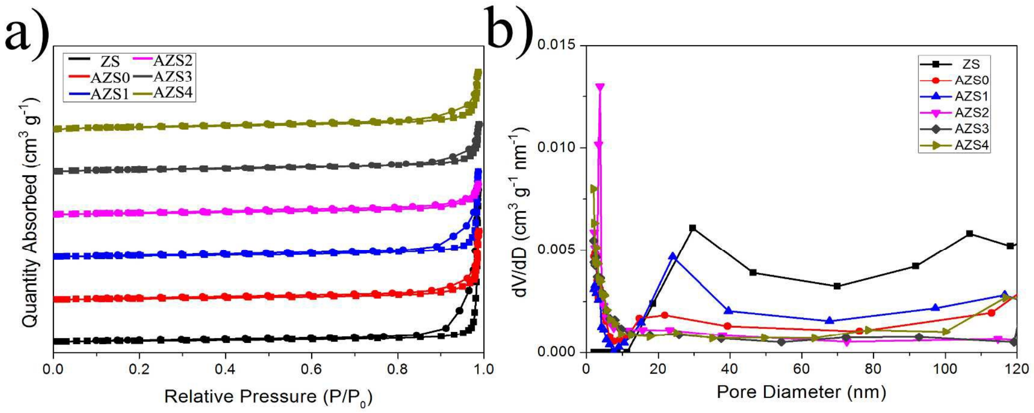

Fig. 5 (a) N_2 adsorption-desorption curves. (b) Pore size distribution plot for the as-prepared Zn_2SnO_4/SnO_2 hollow rounded cubes and Au-Zn_2SnO_4/SnO_2hollow rounded cubes (square symbols: adsorption; circle symbol: desorption).

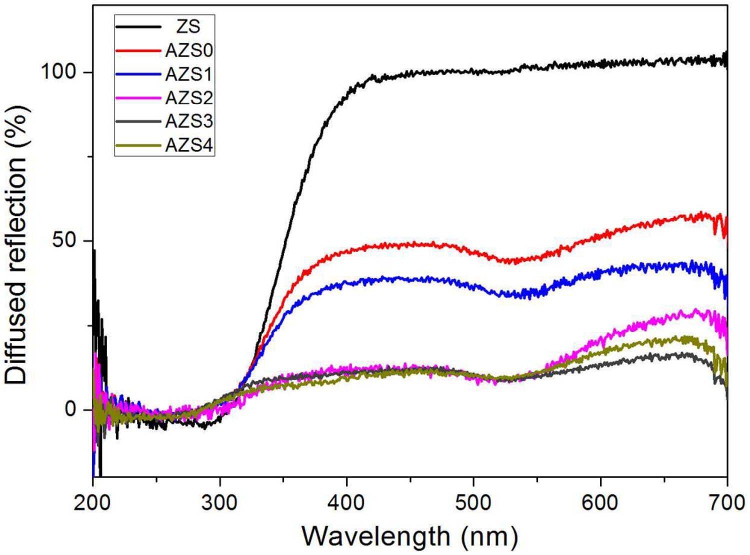

Fig. 6 DRS spectra of ZS, AZS0, AZS1, AZS2, AZS3and AZS4 samples.

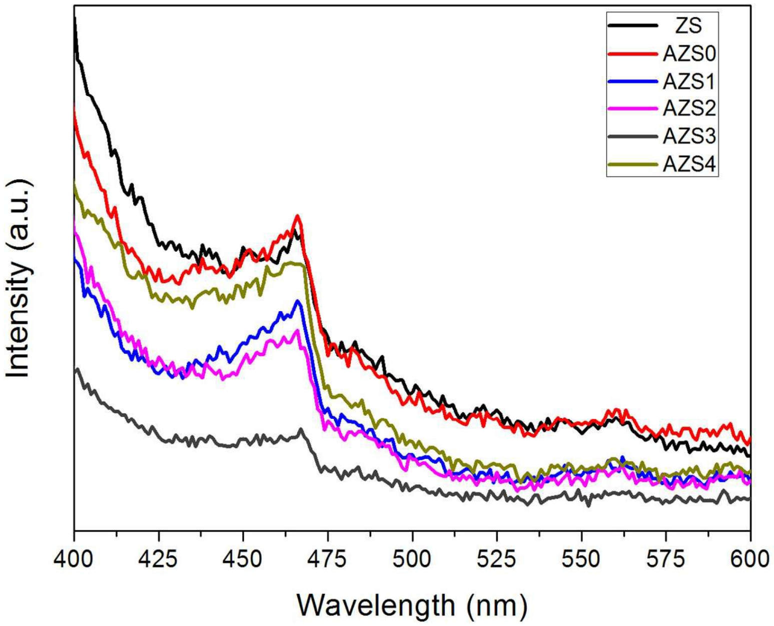

Fig. 7 PL spectra of ZS, AZS0, AZS1, AZS2, AZS3and AZS4 samples.

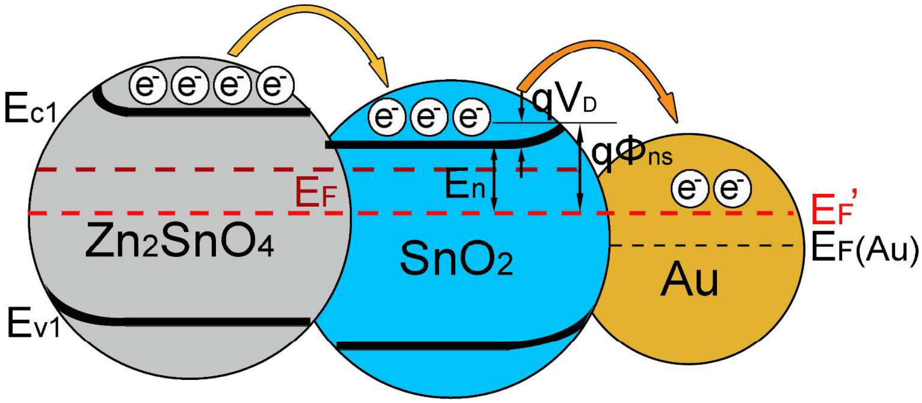

Scheme 1 Charge distribution in semiconductor-metal composites system leads to Fermi level equilibration and potential barrier formation

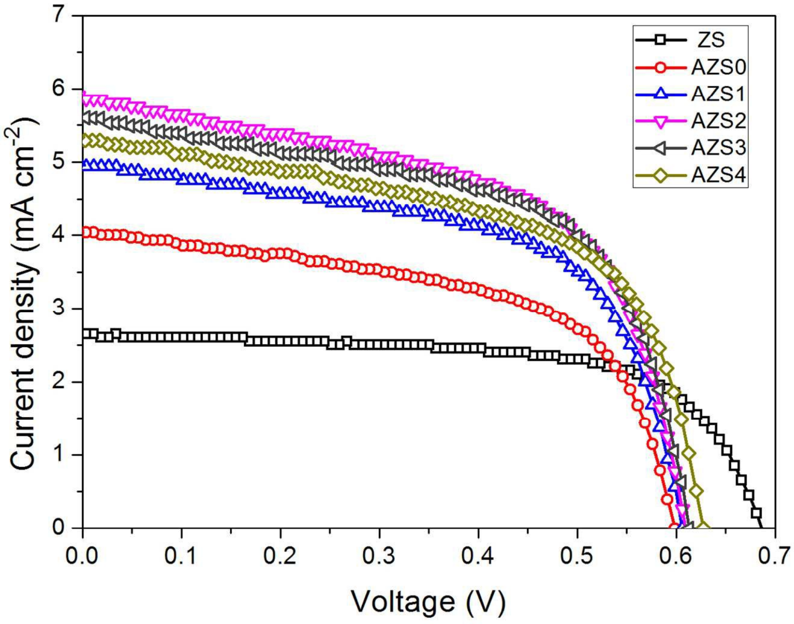

Fig. 8 J-V curves of DSSCs based on samples of ZS, AZS0, AZS1, AZS2, AZS3 and AZS4.

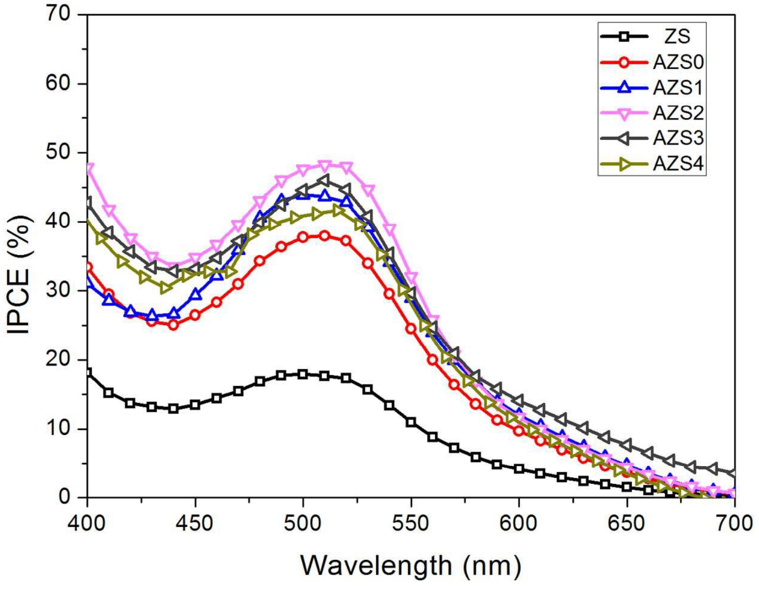

Fig. 9 IPCEspectra of DSSCs based on samples of ZS, AZS0, AZS1, AZS2, AZS3 and AZS4.

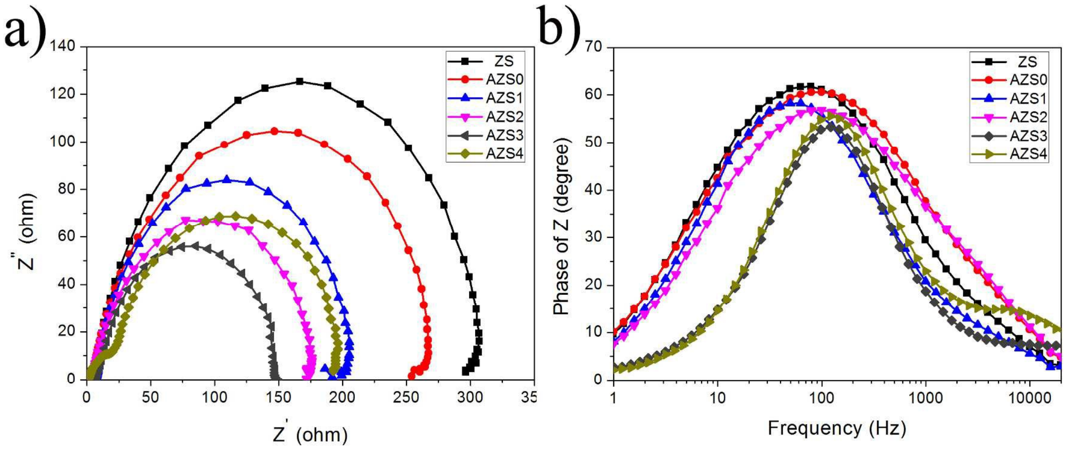

Fig. 10 impedance spectra of DSSCs based on ZS, AZS0, AZS1, AZS2, AZS3 and AZS4photoanodes measured under illumination of 100 mW cm^{-2}: (a) Nyquist plot and (b) Bode phase plots.

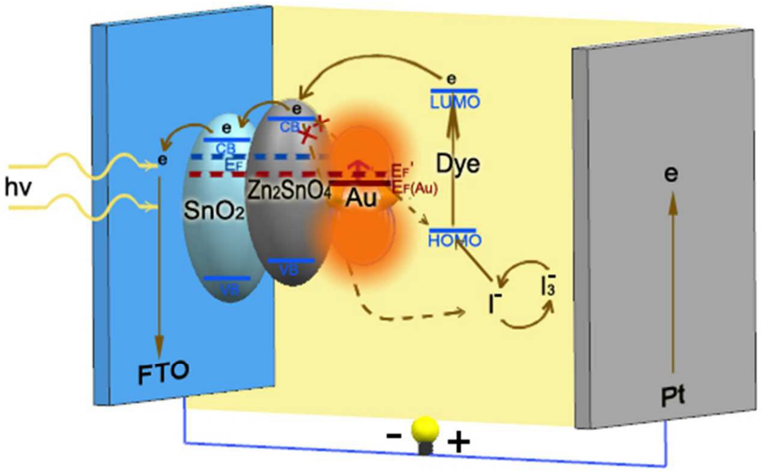

Fig. 11 Schematic illustration of the configuration, surface plasmonic resonance of Au nanoparticles, charge transfer process and adjustment of Fermi level in DSSCs based on Au-Zn_2SnO_4/SnO_2photoanode.